ASTRONOMY & ASTROPHYSICS
SUPPLEMENT SERIES

Astron. Astrophys. Suppl. Ser. **119**, 391-401 (1996)

Photometry of seven clusters of galaxies at intermediate redshift ($z = 0.15 \div 0.50$)*

E. Molinari[1], A. Buzzoni[1,2] and G. Chincarini[1,3]

[1] Osservatorio Astronomico di Brera, Via Bianchi, 46 22055 Merate (Lc), Italy
[2] Visiting astronomer at the INAOE, A.P. 51, 72000 Puebla, Mexico
[3] Università degli Studi, Via Celoria, 16 20133 Milano, Italy
e-mail internet: molinari@merate.mi.astro.it

Received January 11; accepted March 15, 1996

Abstract. — Gunn *g, r, i* photometry for the 7 clusters MRC0254-274, Cl0317+15, MS0418.3-3844, Cl1141-283, A1689, A3594, S0781B is presented. For each cluster we derived the spatial distribution properties obtaining the core radius and the concentration parameters. Color properties of the cluster galaxy population are also briefly discussed.**

Key words: galaxies: clusters: genaral — galaxies: photometry

1. Introduction

There has been recently a renewed interest for the still poorly known distribution of galaxies in clusters and their luminosity function. Biviano et al. (1994), Lopez & Yee (1995) showed, for instance, that the luminosity distribution of the galaxy population seems to correlate with the dynamical age of the cluster. This follows in the same line of previous findings by Melnick & Sargent (1977), and Dressler (1980) of a well recognized correlation between cluster morphology and galaxy population. A proper study towards these goals must include the estimate of the morphology of the member galaxies in addition to their magnitudes and colors, as done by Binggeli et al (1988) for the Virgo cluster. The logical step would then be to compare nearby and distant clusters in order to single out the role of evolution.

In the present work we report a complete three-colors photometry of galaxies in seven clusters spanning a range in redshift from $z = 0.15$ to 0.5. The clusters have been selected from the catalogs of Abell et al. (1989), West & Frandsen (1981), Gunn et al. (1986), Stocke et al. (1991), and McCarthy et al. (1991).

The study of cluster galaxy population is especially suited to characterize early-type population. Among others, such an approach has an important impact on the definition of normal elliptical galaxies as standard candles in some cosmological applications (see e.g. Buzzoni et al. 1993).

2. The data

2.1. *Observations*

CCD observations have been carried out with the 3.6 m ESO telescope at La Silla during several observing runs between 1987 and 1991. The telescope was always equipped with the EFOSC focal reducer providing a projected CCD pixel size of 0.675 arcsec (RCA CCD ESO #3, and CCD ESO#8 and ESO#11 used in 2×2 binned mode) or 0.6075 arcsec (TEK CCD ESO#26). All the observations have been carried out using a dithering technique for best flat-fielding. The whole frame co-addition procedure slightly worsened the image resolution eventually resulting in a PSF FWHM about 2 arcsec. This still allowed however a univocal identification of every object present in all the three photometric bands.

The Gunn system (Thuan & Gunn 1976; Wade et al. 1979) has been chosen for full compatibility with our previous work in order to build up an homogeneous database (Molinari 1993; Molinari et al. 1990, 1994a,b).

In Fig. 1 we show the cluster fields after coadding all the images in the three filters. Table 1 lists the cluster parameters as collected in the literature. Astrometry has been performed using the grid of GSC stars in the field of the POSS digitalized plates. Cluster fiducial coordinates were chosen to coincide with a convenient bright object

Send offprint requests to: E. Molinari
*Based on observations made at the European Southern Observatory (ESO), La Silla, Chile
**Tables 3 to 9 are available in electronic form via anonymous ftp at the CDS (130.79.128.5)

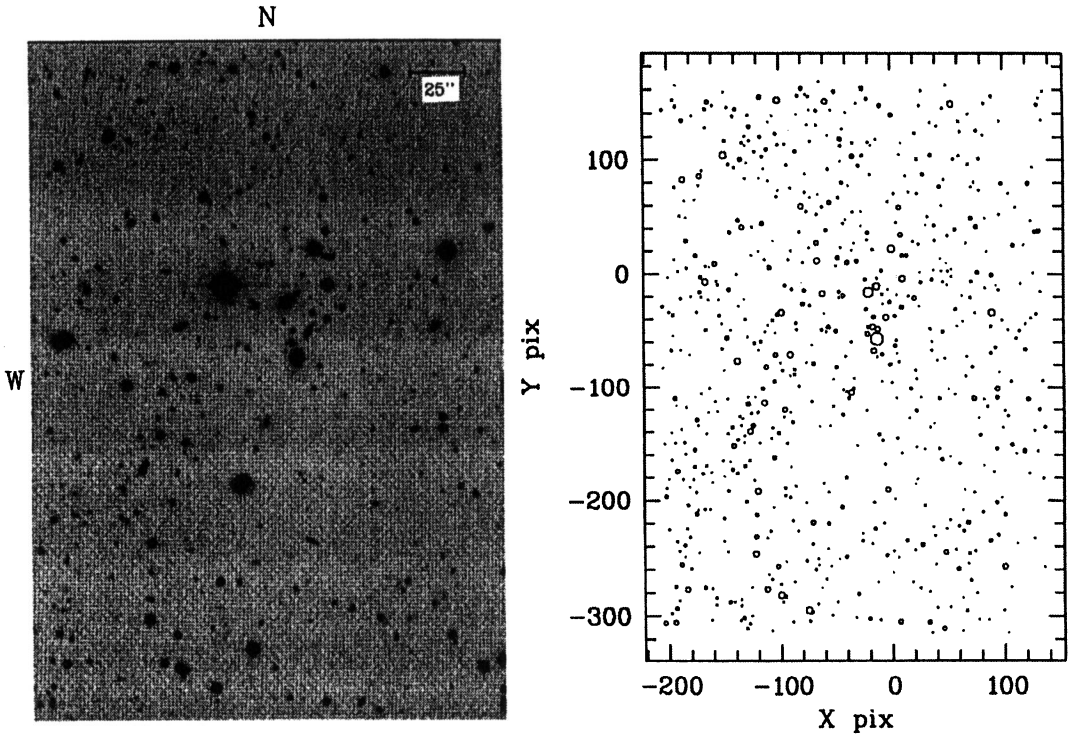

Fig. 1. a) Composite g, r, i image of MRC0254−274 and X, Y plot of the photometric catalog

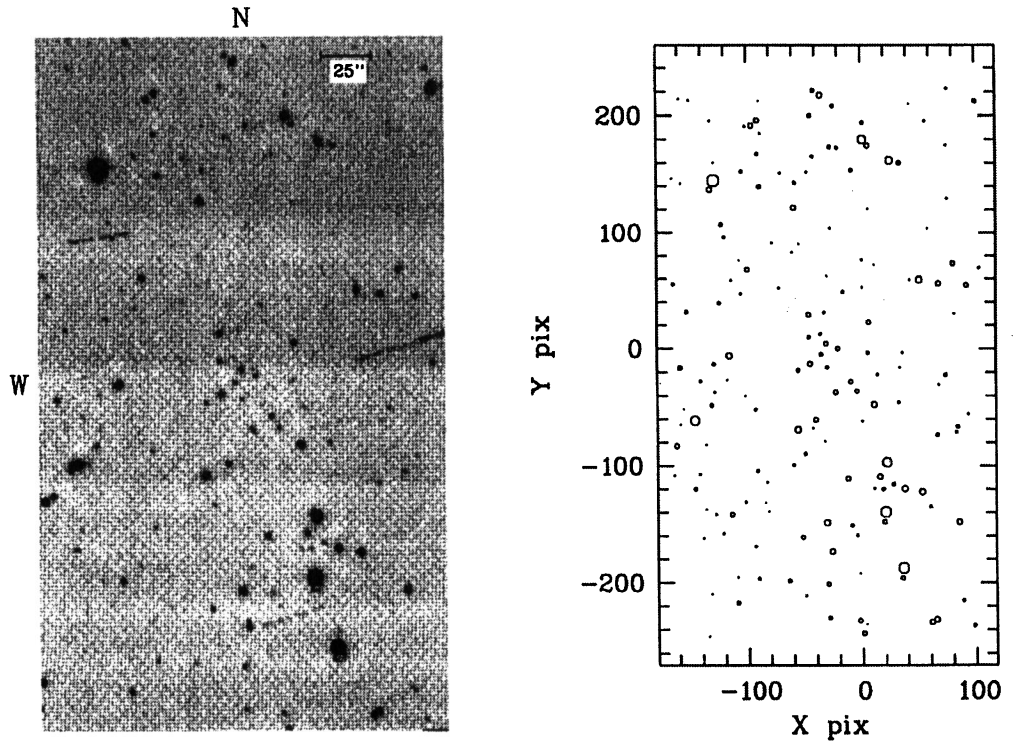

Fig. 1. b) Composite g, r, i image of Cl0317+15 and X, Y plot of the photometric catalog

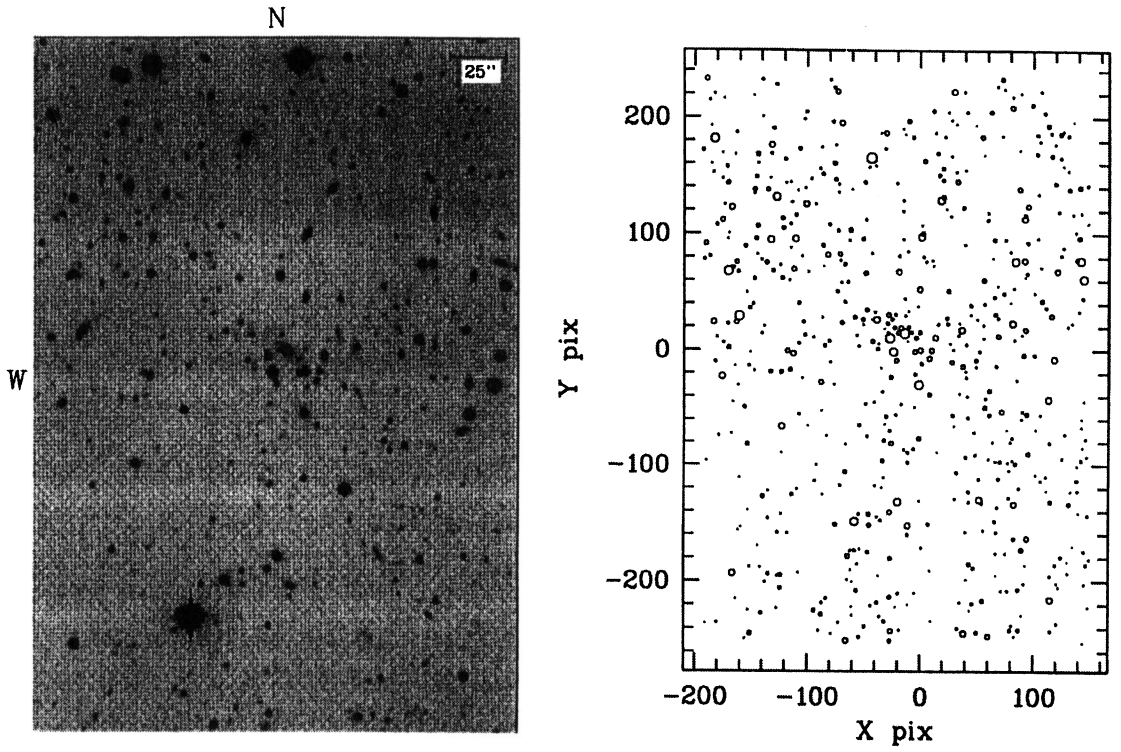

Fig. 1. c) Composite g, r, i image of MS0418.3−3844 and X, Y plot of the photometric catalog

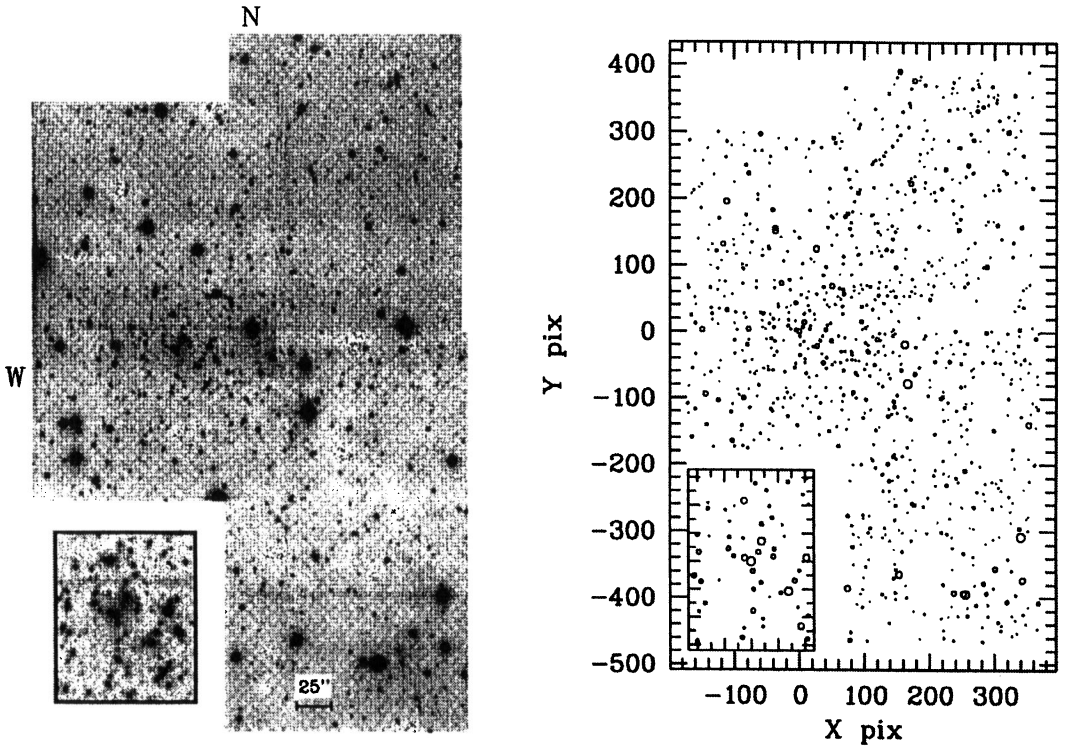

Fig. 1. d) Composite g, r, i image of Cl1141−283 and X, Y plot of the photometric catalog (with core area enlargment)

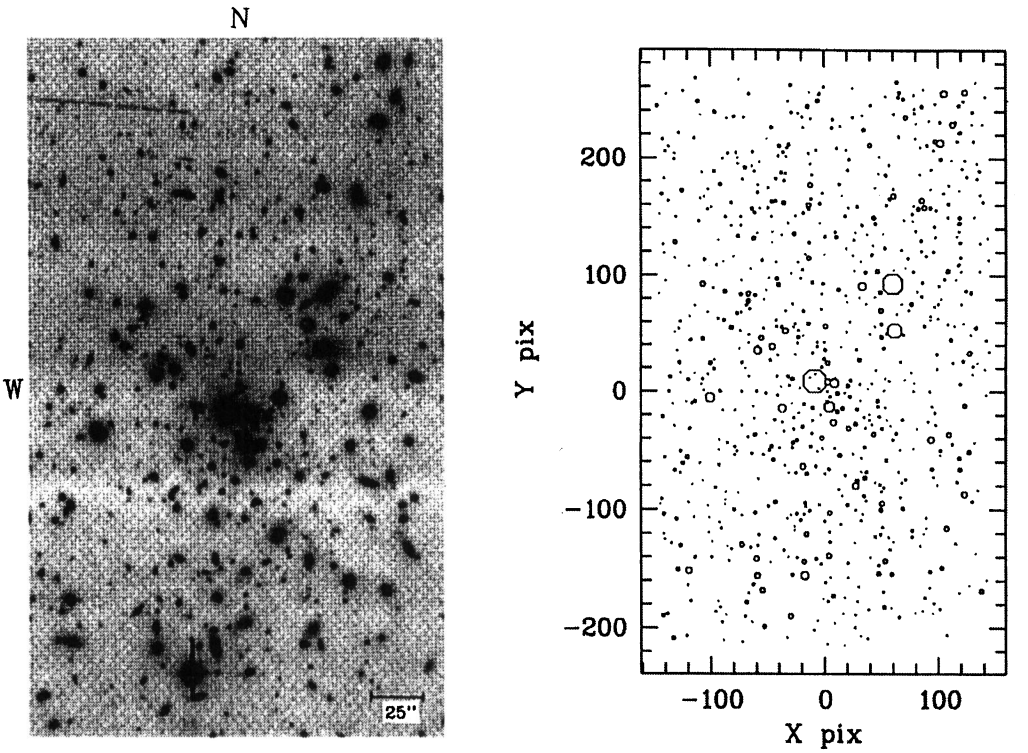

Fig. 1. e) Composite g, r, i image of A1689 and X, Y plot of the photometric catalog

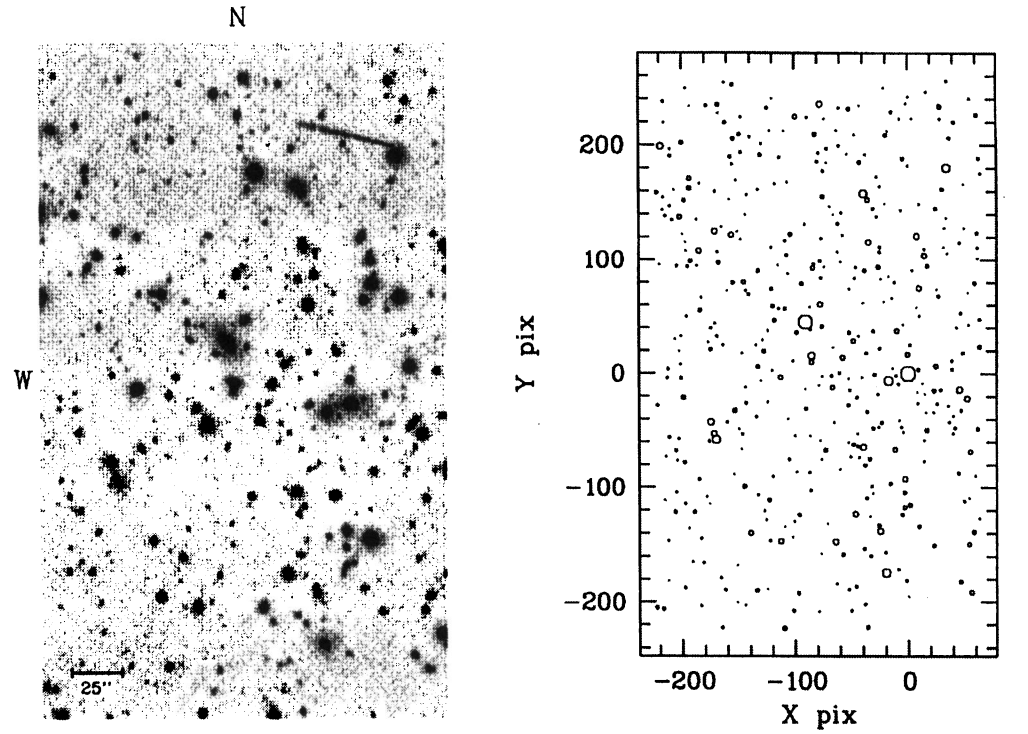

Fig. 1. f) Composite g, r, i image of A3594 and X, Y plot of the photometric catalog

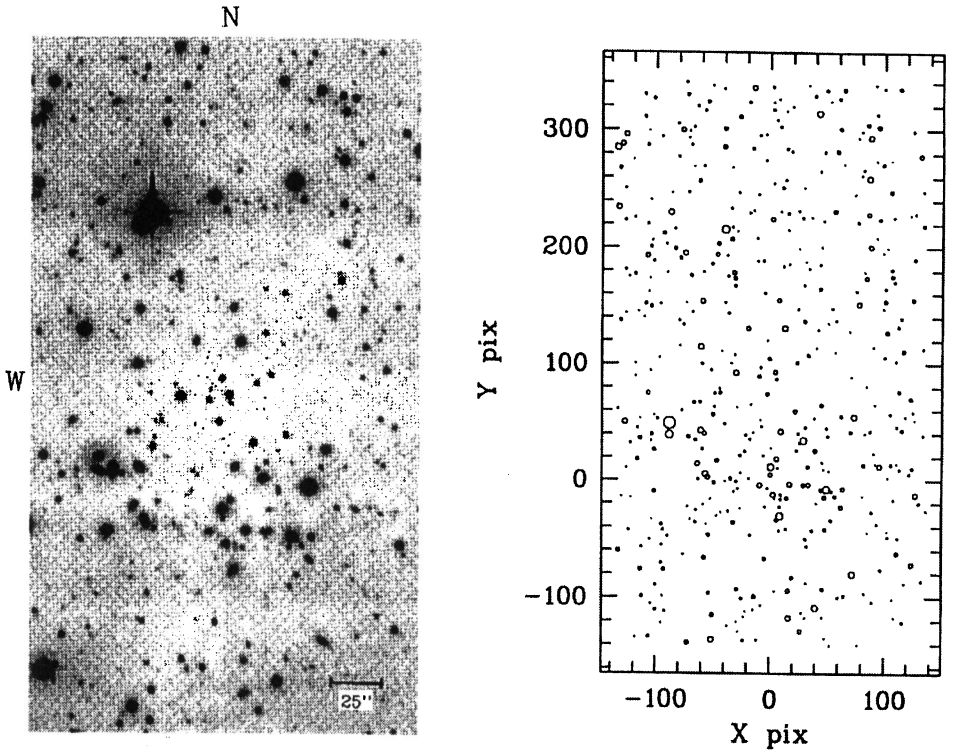

Fig. 1. g) Composite g, r, i image of S0781B and X, Y plot of the photometric catalog

near the center, identified in Table 1 by its catalogue number (cf. Sect. 3). In Table 2 we report the journal of observations along with the relevant photometric parameters of the reduced images.

2.2. *Redshifts*

Some of the clusters in our sample have also been observed spectroscopically with EFOSC obtaining low-dispersion MOS spectra for 83 galaxies at a nominal resolution of 14 Å FWHM at 5000 Å. For three clusters, MRC0254-274, MS0418.3-844 and Cl1141-283 (see Table 1) we derived an accurate value of the redshift, while for A1689 we adopted $z = 0.1847$ according to Teague et al. (1990). The redshift distribution of the objects in Cl0317+15 is rather broad supporting the possibility of a prospectic clump of galaxies at distances between $z = 0.27$ and 0.40.

A full discussion of the spectroscopic data will be the subject of a next paper in this series (Longhetti et al. 1996).

2.3. *Photometric calibration*

The basic image processing relied on a dithering technique for the flat-fielding procedure using the same science exposures. The procedure is fully standard and consists of taking different exposures of each field by slightly tilting the telescope after each image. The total set of frames is then combined by assigning each CCD pixel its median value of the signal. This assures an almost perfect match of the true sky background level and fringe pattern. The sky rms after the whole cleaning procedure was thus always below 1% with a typical value of about 0.5%.

The standard stars used for magnitude calibration were selected from the list of Thuan & Gunn (1976) and Wade et al. (1979). The absolute zero-point error in the photometry is below 0.05 mag for all of the clusters observed in the various filters and no systematic offsets seem to appear. Therefore, magnitudes are mainly affected by the internal Poissonian scatter such as $\sigma \propto 10^{0.2(\mathrm{mag})}$. The typical uncertainty is 0.2 mag for objects about magnitude 22.

The frames named Field 2 and Field 3 in the photometry of the clusters Cl1141-283 (obtained during different observing runs, see Table 2) were calibrated on the basis of the magnitude of the objects in the overlapping area with Field 1. The scatter plot of the magnitude differences of the common objects is given in Fig. 2, allowing a direct measure of the Poissonian error in the photometry.

Object detection and magnitude estimate were performed using the INVENTORY package (West & Kruszewsky 1981) as implemented in the ESO MIDAS environment. The detection threshold (used also as limiting isophote for the isophotal magnitudes) was set up to 1% of the sky level for the two clusters Cl0317+15 and Cl1141-283 (namely five magnitudes fainter than the sky

Table 1. Relevant clusters parameters

Name	Coord. (J2000) α	δ	l	b	Ref Obj No.	z	m–M (1)	T_{BM} (3)	E_{B-V} (4)	Ref. (5)
MRC0254-274	$02^h56^m52^s$	−27°17′51″	220.6	−62.2	477	0.480	42.76	II	0.00	MCC
Cl0317+15	$03^h20^m03^s$	+15°17′51″	167.6	−34.2	109	–	42.30:	III	0.14	GHO
MS0418.3-3844	$04^h20^m05^s$	−38°38′11″	241.6	−45.3	299	0.339±0.001	41.88	II	0.01	EMS
Cl1141-283	$11^h44^m09^s$	−28°35′08″	285.5	+32.0	536	0.5012±0.0009	42.87	II-III	0.08	WF
A1689	$13^h11^m29^s$	−01°20′51″	313.3	+61.1	308	0.1847	40.42	I-II	0.01	ACO
A3594	$14^h20^m22^s$	−17°44′48″	331.1	+40.2	199	(2)	–	II	0.07	ACO
S0781B	$15^h00^m15^s$	−18°08′19″	341.1	+35.0	162	(2)	–	III:	0.10	ACO

Notes to the table:
(1) m–M = $5log\ d_L + 25$ with d_L the luminosity distance in Mpc from z with the adopted cosmology;
(2) distance class 6 clusters from ACO catalog;
(3) Bautz-Morgan class;
(4) from Burstein and Heiles (1982).
(5) MCC = McCarty et al., 1991; GHO = Gunn et al., 1986; EMS = Stocke et al., 1991; WF = West and Frandsen, 1981; ACO = Abell et al., 1989

Table 2. Journal of observations

cluster	filter	date	CCD ESO#	total exp time (″)	frames (no.)	mag lim (1)	objects (no.)	(2)	sky brigth. (mag arcsec^{-2})	sky rms (%)	PSF (arcsec)
MRC0254-274	g	28.Nov.91	26	2700	3	26.0	704	total 755	22.24	0.6	1.6
	r	28.Nov.91	26	2700	3	26.0	662	*gri* 408	21.51	0.4	1.7
	i	28.Nov.91	26	2700	3	24.5	423		20.20	0.3	1.6
Cl0317+15	g	20.Nov.87	3	3000	5	26.0	203	total 270	21.94	0.4	2.2
	r	21.Nov.87	3	2400	4	25.5	167	*gri* 97	21.33	0.3	2.9
	i	21.Nov.87	3	2400	4	24.0	134		19.79	0.2	2.5
MS0418.3-3844	g	29.Nov.91	26	2700	3	25.5	527	total 636	21.47	0.5	1.8
	r	29.Nov.91	26	2700	3	25.5	567	*gri* 330	20.96	0.4	1.9
	i	29.Nov.91	26	2700	3	24.5	374		19.78	0.3	2.1
Cl1141-283/1	g	18.Apr.90	8	2880	4	25.0			23.32	0.4	2.1
	r	18.Apr.90	8	3600	5	24.0	all fields		22.65	0.3	2.1
	i	18.Apr.90	8	2160	3	24.0			21.38	0.3	2.3
Cl1141-283/2	g	18.Apr.90	8	1800	3	25.0	879	total 1109	22.91	0.5	2.0
	r	18.Apr.90	8	1800	3	24.5	883	*gri* 568	22.27	0.4	2.2
	i	18.Apr.90	8	1800	3	24.0	721		21.29	0.3	2.2
Cl1141-283/3	g	16.Apr.91	8	2100	3	25.0			21.24	0.6	2.0
	r	16.Apr.91	8	1800	3	24.5			20.65	0.5	1.7
	i	16.Apr.91	8	2400	3	24.0			20.06	0.3	1.7
MRC0254-274	g	28.Nov.91	26	2700	3	26.0	704	total 755	22.24	0.6	1.6
	r	28.Nov.91	26	2700	3	26.0	662	*gri* 408	21.51	0.4	1.7
	r	28.Nov.91	26	2700	3	24.5	423		20.20	0.3	1.6
A1689	g	16.Apr.91	8	2700	3	25.0	775	total 840	21.48	0.3	2.0
	r	16.Apr.91	8	2700	3	25.0	747	*gri* 605	21.00	0.2	2.1
	i	16.Apr.91	8	2700	4	25.0	634		20.26	0.2	1.9
A3594	g	19.Apr.91	8	2700	3	24.5	378	total 455	21.19	0.2	1.8
	r	19.Apr.91	8	2700	3	25.0	417	*gri* 299	20.89	0.2	1.8
	i	19.Apr.91	8	2700	3	24.0	347		20.03	0.2	1.7
S0781B	g	17.Apr.91	8	2700	3	25.0	455	total 521	21.51	0.3	1.4
	r	17.Apr.91	8	2700	3	25.0	454	*gri* 303	21.09	0.4	1.8
	i	17.Apr.91	8	2700	3	25.0	343		20.24	0.3	1.6

(1) Defined as the faint magnitude bin where the counts of the LF drops to 50%.
(2) The total set of objects is the union of the 3 filters sets, *gri* denotes the intersection.

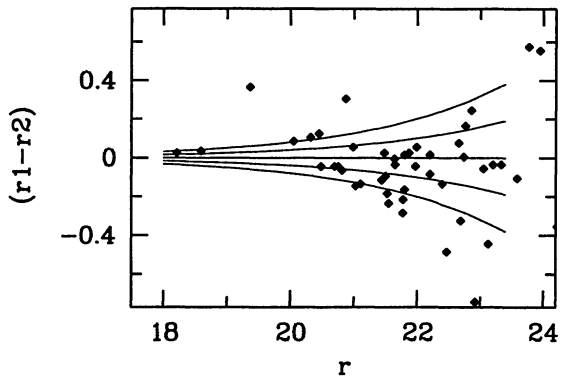

Fig. 2. Differences in the magnitude determination of the objects in common in the different fields of Cl1141-283. Solid lines show a Poissonian error prediction for $\sigma(r = 22) = 0.1$ and 0.2 mag

brightness reported in Table 2), while a lower value of 0.5% was adopted in the others taking advantage of a better flat-fielding. From the photometric procedure were excluded the saturated stars and the many(!) asteroid trails, which are clearly seen in the pictures of Fig. 1 (see Molinari et al. 1996 for more details about these, mostly new, objects).

A local sky-level determination as used in the INVENTORY package is well suited for a flat background and works well also in presence of low-frequency spatial variations. The presence of bright, extended objects (such as D or cD galaxies in the cluster cores) introduces some complications leading to a poor determination of the photometric properties of the nearby fainter objects. We had then to devise a modelling procedure in order to subtract the light from the brightest sources and apply the INVENTORY procedure on the CCD frames with objects that were comparable in size (mostly seeing limited images).

The actual method consisted in extracting the intensity profiles along circular path, centered on the galaxy position, with radius several tenths of pixels from the center, depending on the actual object size. All these 'circular' profiles were then fitted with few terms of a Fourier series, allowing even terms to be present only in the innermost radii. In this way any ellipticity, and also a small value of the decentering of the galaxy were taken into account in a straightforward way. The fitting procedure was iterated 3-4 times eliminating the pixels with a k–σ clipping. The model thus obtained was replaced in the profile wherever the observed differed by more than $k \cdot \sigma$. Subtraction of these modified 'circular' profiles leaves the superimposed (smaller) objects untouched in the frame.

3. Catalogs

In Fig. 1 (right panels, a to g) all the objects detected in the field are plotted scaling with their r-isophotal radius. Tables 3-9[1] give the complete photometric catalogs of the seven cluster fields. The columns of Tables 3-9 read as follows: (1) the *ID number* of the object; (2) its X and Y coordinates, in pixels, with respect to the adopted center (cf. Sect. 4.2); (3) the *g, r, i isophotal magnitudes* each computed down to the threshold quoted in the previous section; (4) the $g-r$ and $g-i$ colors computed through a 3 or 5 pixel aperture photometry, depending on the computed r isophotal radius but kept fixed for each filter; (5) the *isophotal radius* in the r band in pixels (when available)

4. Data analysis

4.1. *Completeness*

The completeness of the photometric catalogs is limited at faint magnitude by crowding. A bootstrap test has been performed by spreading throughout the cluster image a grid of real stars rescaled to different apparent magnitudes from 18 to 26. The test, applied to the r image of the cluster A3594, gave 90%, 50% and 10% efficiency of detections at r=22.5, 24.0 and 25.0, respectively. The test was performed on the raw image, without the exclusion of the bright, extended objects, so that the efficiency of the detection represents the real situation. The limiting magnitude quoted in Table 2 refers to a 50% incompleteness level in the apparent luminosity function.

4.2. *Spatial distribution*

An object density map was used to determine the position of the center of the clusters. The adopted center marks the highest density peak and has been chosen as the local (0,0) origin point of our coordinates in the photometric catalogs of Tables 3-9. Incidentally, note that, although very close, this is not exactly the position of the bright object used for the astrometry in Table 1.

The mean surface profile of the clusters has been modeled with a King profile. The actual procedure consisted in smoothing the apparent object density just to derive a mean surface radial profile for each cluster, averaged over 36 equally spaced slices by centering on the cluster core. With this procedure, error bars are simply a measure of the anisotropy in the cluster shape. The mean profile was then fitted with a function such as

$$\sigma(r) = \sigma_0/(1 + r/R_c^2)^{3\beta-\frac{1}{2}} + \sigma_B, \qquad (1)$$

where the surface density $\sigma(r)$ depends on the four parameters σ_0 (the central surface density of the cluster),

[1]Tables 3 to 9 are available in electronic form via anonymous ftp at the CDS database.

R_c (the core radius), a concentration index β and σ_B (the background object density).

The parameter β is a measure of the deviation from an isothermal sphere (for which $\beta = 1$ in the King (1962) approximation), and can be related to the C concentration index used by Butcher & Oemler (1984). Thus, $\beta \sim 1$ (isothermal distribution) corresponds to $C \sim 0.7$; $\beta < 1$ (broader profile) to higher values of C; $\beta >> 1$ (concentrated clusters) to low values of C, down to the homogeneous sphere with very high values of β and $C \sim 0.3$.

Table 10 summarizes the fitting parameters. A marker in the last column of the table means that no satisfactory isotropic model can be found in the χ^2_ν space to fit the data. In this case values are to be regarded only as a rough estimate of the size of the cluster core. A similar warning also applies to the determination of the background σ_B. In fact, at lower redshift clusters overflow the CCD field of view. This means therefore that all the parameters quoted in Table 10 more properly represent a modelling of the core density enhancement.

The numbers in parenthesis near the values of σ_B are a crude estimate of the number counts predicted by the survey of Driver et al. (1994), after a straightforward translation from their color system to our one, assuming a mean color of our sample as derived from the visual inspection of the field color-magnitude diagrams (see next section). This simplification introduces of course a large uncertainty in the predicted counts, between 20 and 50% depending on the passband. Neuschafer & Windhorst (1995) also translated Tyson's (1988) CCD counts to the Gunn system estimating a field density of $\sim 6\ 10^4$ galaxies per square degree down to $r = 24.5$.

From our data, after rescaling for the secant dependence on galactic latitude (Jarvis & Tyson 1981), we systematically derive a somewhat higher density, in excess of a factor of 1.5 with respect to Driver et al.'s (1994) counts and a factor of two with respect to Neuschafer & Windhorst (1995). This excess might be partially recovered by accounting for the uncertainty in the precise magnitude limit.

As a general trend, the field around poor aggregations displays a lower density (Cl0317+15 and S0781B). This might be due to the fact that the density of field galaxies is higher in the neighborhood of clusters and, perhaps, to contamination by the cluster outskirt.

4.3. *Color properties*

Figure 3 (left panels) displays the r vs. $g - r$ diagram of all the catalog entries of Tables 3-9. The ridge line of the color-magnitude ($c - m$) relation for the ellipticals (Visvanathan & Sandage 1977) clearly appears, especially for the most compact clusters MS0418, A1689, and A3594 thanks also to a larger galaxy statistics. Striking is the case of Cl1141-283, the most distant cluster in our sample ($z = 0.5012$), showing a smeared sequence of early-type galaxies due to a nearer concentration of ellipticals at $z = 0.21$ according to our spectroscopy.

In all of the cases but for MRC0254-274, the c-m relation becomes sharper when accounting only for the objects in the central region of the clusters (within 1–2 core radii, cf. the right panels of Fig. 3). This is in agreement with the well recognized evidence of galaxy morphological segregation (Dressler 1980). Even the case of MRC0254-274 can be easily understood in this sense as the cluster is in fact a loose clump of galaxies embedded in a high-density (elliptical-dominated) field.

The presence of 'blue' galaxies with respect to the locus of the cluster ellipticals in the c-m diagram (cf. the right panels in Fig. 3) might be regarded as a signature of the Butcher & Oemler (1984) effect. This effect foresees the fraction of blue galaxies in clusters to increase with redshift, but its operational definition (Butcher & Oemler 1984) and the low number of objects usually involved in the measurements (Newberry et al. 1988; Molinari 1993) always made the error bars so large that scarce information could be obtained from purely photometric studies, which led anyway to the more quantitative spectroscopic surveys (Dressler & Gunn 1982). Therefore we do not attempt to give a statistical unreliable measurement of the blue-galaxy fraction in our cluster, just noting that only the farthest cluster Cl1141-283 shows blue galaxies among the core objects marked in Fig. 3.

According to Buzzoni et al. (1993), a two-color diagram is a useful tool to pick up the cluster elliptical galaxy population at different redshift as shown in Fig. 4 using a $g - r$, $g - i$ diagram. The clump due to the early-type galaxies is more evident for the more compact clusters. For comparison, the expected path in the color diagram with increasing redshift for an elliptical galaxy template model from Buzzoni (1995) is reported in the lower right panel.

The identification of other classes of objects is not a simple task in our photometry. Actually, seeing limitation does not allow us to perform any deep morphologically-based star/galaxy and bulge/disk-system separation. We only notice the paucity of stellar contamination, as stars would only populate the upper left corner of the color-color plane. In addition, the objects which show a color bluer than the elliptical concentration cannot in principle be splitted into their two components of the late-type cluster galaxies and a mix of foreground interlopers. The nature of the reddest objects in the $g - r$, $g - i$ plane is usually adscribed to background early-type galaxies, as only this morphological type can achieve such red colors at any redshift, but the 'bifurcation', which in the two panels of Cl1141-283 and S078B splits in two the objects redder than $g - r \geq 1.2$ and $g - i \geq 1.6$ may arise a series of questions on the different nature of cluster and field ellipticals, and repropose the question of the presence of

Table 10. Spatial distributions of galaxies

Name	σ_0 10^4 obj/deg^2	R_c(1) pixel	Mpc	σ_B(2) 10^4 obj/deg^2	β(3)	fit(4)
MRC0254-274	12.6	27	0.13	13.6 (6.5)	0.72	
Cl0317+15	6.1	15	0.07:	6.0 (7.5)	17.1	
MS0418.3-3844	16.7	16	0.06	13.1 (7.5)	11.9	
Cl1141-283	17.0	28	0.15	6.2 (3.8)	0.68	no
A1689	18.5	35	0.10	12.3 (7.5)	0.79	
A3594	10.1	21	-	9.0 (4.5)	1.22	no
S0781B	13.9	23	-	9.1 (7.5)	1.26	

Notes:
(1) defined as R_c where the $\sigma(R_c) = 0.5\sigma_0$
(2) in parenthesis the predicted counts from Driver et al. (1994)
(3) concentration parameter
(4) is *no* when the $\chi^2_\nu > 2.0$
all numbers are quoted up to the last significant digit

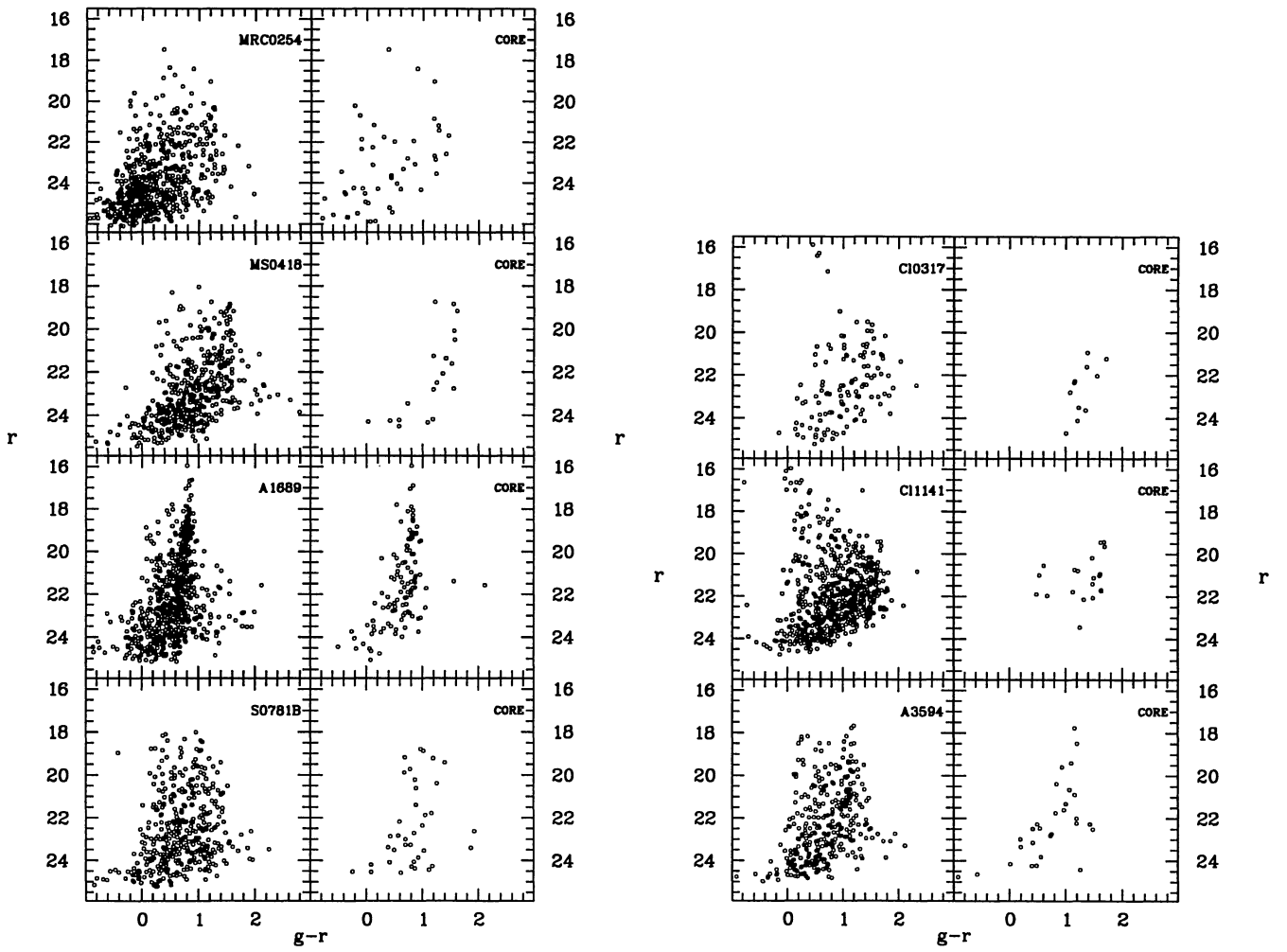

Fig. 3. Color-magnitude diagrams for all the clusters. In the left panels all objects with $g-r$ color are plotted, while in the right panels only the objects within $1-2$ $R_{\rm core}$ are present. The dominance of the ellipticals obeying the $c-m$ relation is evident

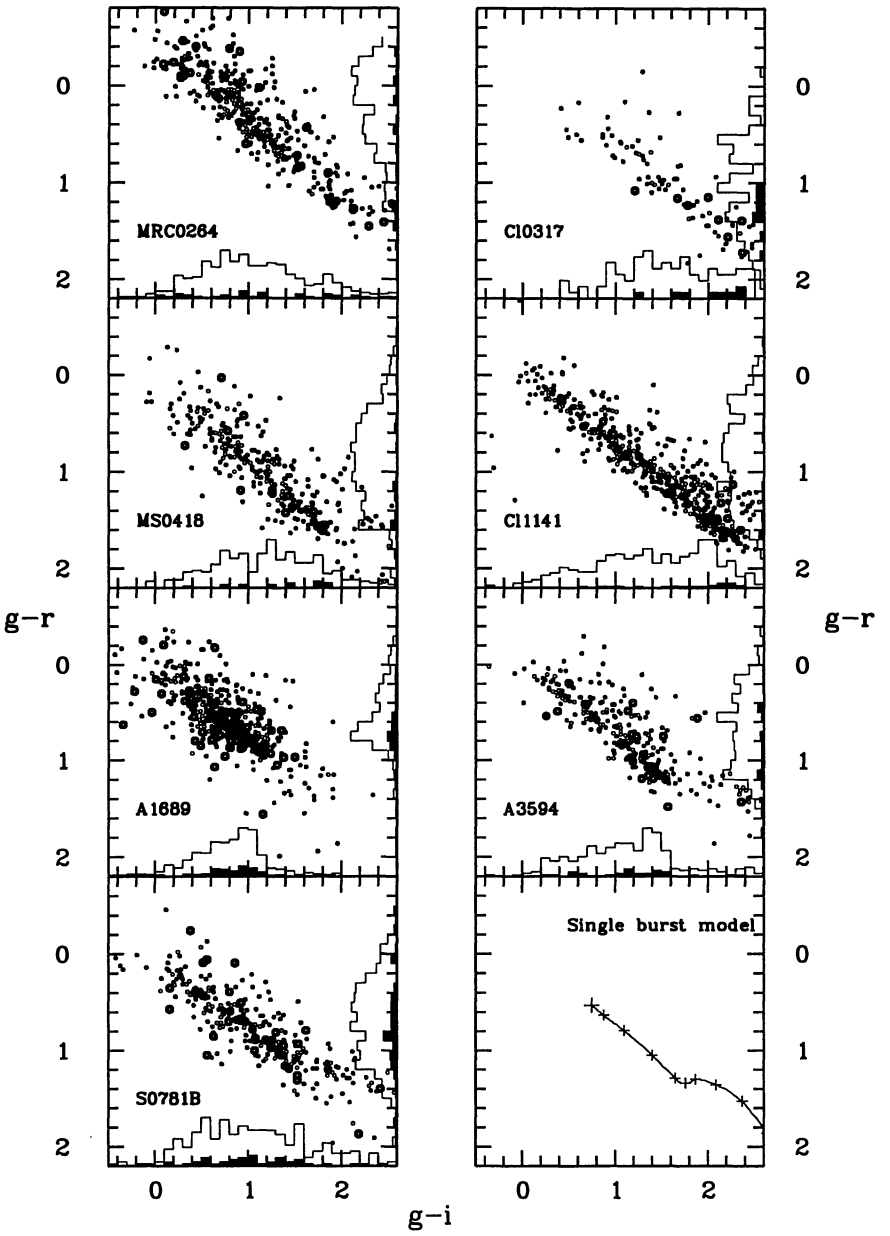

Fig. 4. Color-color plots for the 7 clusters. The open histograms on the axis show the color distributions in $g-i$ and $g-r$ of all the objects. the filled histogram and the bigger circles evidence the core objects (see right panels in Fig. 3). In the lower right panel the predicted color for a model elliptical are plotted (Buzzoni 1995), with a cross marking every 0.1 step in redshift. Local ($z = 0$) galaxies are represented by the bigger cross

objects showing an i excess (Garilli et al. 1995; Molinari et al. 1994b).

In another paper, the possibility of extracting morphological information using multicolor photometry will be further explored, testing the consistency of a classification based only on photometric data making use of artificial intelligence (Molinari 1995).

References

Abell G.O., Corwin H.G. Jr, Olowin R.P., 1989, ApJS 70, 1
Binggeli B., Sandage A., Tamman G.A., 1988, ARA&A 26, 509
Biviano A., Durret F., Gerbal D., et al., 1995, A&A 297, 610
Burstein D., Heiles C., 1982, AJ 87, 1165
Butcher H., Oemler A., 1984, ApJ 285, 426
Buzzoni A., 1995, ApJS 98, 69
Buzzoni A., Chincarini G., Molinari E., 1993, ApJ 410, 499
Dressler A., 1980, ApJ 236, 351
Dressler A., Gunn J.E., 1982, ApJ, 263, 533
Driver S.P., Phillipps S., Davies J.I., Morgan I., Disney M.J., 1994, MNRAS 266, 155

Garilli B., Maccagni D., Carrasco L., Recillas E., 1995, in: proceedings of "Fresh Views of Elliptical Galaxies". In: Buzzoni A., Renzini A., Serrano A. (eds.) ASP: San Francisco, p. 297
Gunn J.E., Hoessel J.G., Oke J.B., 1986, ApJ 306, 30
Jarvis J.F., Tyson J.A., 1981, AJ 86, 476
King C.R., 1962, AJ 67, 471
Longhetti M., Buzzoni A., Chincarini G., Molinari E., 1996 (in preparation)
Lopez O., Yee H.K.C., 1995, in: proceedings of "Fresh Views of Elliptical Galaxies". In: Buzzoni A., Renzini A., Serrano A. (eds.), ASP: San Francisco, p. 279
McCarthy P.J., van Bruegel W., Kapahi V.K., Subrahmanya C.R., 1991, AJ 102, 522
Melnick J., Sargent W.L.W., 1977, ApJ 215, 401
Molinari E., 1993, Ph.D. Thesis dissertation, Univ. of Milano
Molinari E., 1995, in: proceedings of "Fresh Views of Elliptical Galaxies". In: Buzzoni A., Renzini A., Serrano A. (eds.), ASP: San Francisco, p. 275
Molinari E., Buzzoni A., Chincarini G., 1990, MNRAS 246, 576
Molinari E., Banzi M., Buzzoni A., Chincarini G., Pedrana M.D., 1994a, A&AS 103, 245
Molinari E., Buzzoni A., Chincarini G., Pedrana M.D., 1994b, A&A 292, 54
Molinari E., Buzzoni A., Carpino M., 1996, A&A (in preparation)
Neuschafer L.W., Windhorst R.A., 1995, ApJS 96, 371
Newberry M.V., Kirshner R.P., Boroson T.A., 1988, ApJ 335, 629
Stocke J.T., Morris S., Gioia I., et al., 1991, ApJS 76, 813
Teague P.F., Carter D., Gray P.M., 1990, ApJS 72, 715
Thuan T.X., Gunn J.E., 1976, PASP 88, 543
Tyson J.A., 1988, AJ 96, 1
Visvanathan N., Sandage A., 1977, ApJ 216, 214
Wade R.A., Hoessel J.G., Elias J.H., Huchra J.P., 1979, PASP 91, 35
West R.M., Frandsen J., 1981, A&AS 44, 329
West R.M., Kruszewski A., 1981, Irish Astron. J. 15, 25